International Journal of ISSI, Vol. 22(2025), No. 2, pp. 83-90

Online ISSN: 2981-0396 Print ISSN: 2981-0388

International Journal of Iron & Steel Society of Iran

Journal Homepage: https://journal.issiran.com/

Research Article

Microstructural and Mechanical Properties of a Medium-Silicon Low-Alloy Steel under Quenching and Partitioning Heat Treatment: A Comparative Study with Step Quenching Process

A. Khajesarvi *[1], S. S. Ghasemi Banadkouki [2]

Department of Mining and Metallurgical Engineering, Yazd University, Yazd, Iran

ARTICLE INFO

Keywords:

Medium-Silicon Low-Alloy Steel, Quenching and Partitioning (QP), Step Quenching (SQ), Mechanical Properties.

Article history:

Received 02 September 2025
Received in revised form 28 September 2025
Accepted 25 July 2026

ABSTRACT

This study aims to investigate the mechanical behavior of a medium-silicon low-alloy steel subjected to quenching and partitioning (QP) heat treatment and to compare it with that of step quenching (SQ). Microstructural observations were carried out using field-emission scanning electron microscopy (FE-SEM) with electron backscatter diffraction (EBSD) and transmission electron microscopy (TEM). Furthermore, mechanical tests including hardness, tensile, and impact tests, as well as phase analysis by X-ray diffraction (XRD), were employed. The results revealed that the product of ultimate tensile strength and total elongation, a reliable criterion for evaluating advanced high-strength steels, increased from 2.4 to 10.2GPa·% in QP samples at 280°C, compared with SQ samples at 720°C. The improvement in the mechanical properties of QP specimens is attributed to a micro-composite microstructure containing carbide-free tempered martensite (CFTM), fresh martensite (FM), carbide-free bainite (CFB), and retained austenite (RA). This differs from the ferrite–martensite dual-phase microstructures of SQ specimens. Moreover, the Charpy impact energy of SQ specimens was 3.5J, while the QP specimens exhibited the highest impact energy absorption with 5.5J.

1. Introduction

Advanced high-strength steels (AHSS) have been extensively investigated to achieve an optimal combination of mechanical properties and toughness while simultaneously reducing production costs [1, 2]. These investigations have been carried out in particular in the automotive industry to address concerns about reducing the weight of steel components to save energy and raw materials [3, 4]. Dual-phase (DP) steels exhibit desirable mechanical properties, including high tensile strength and a high work-hardening rate [4]. These favorable properties are attributed to their microstructural characteristics, in which the soft ferritic matrix ensures adequate ductility, while the harder phase (bainite or martensite) provides load-bearing capability [5]. One of the heat-treatment cycles used to obtain a dual-phase microstructure is SQ. In the SQ process, the steel is heated to the single-phase austenite region. After complete austenitization, it is transferred into a molten salt bath at

* *Corresponding Author*
Email: alikhajesarvi@yahoo.com
Address: Department of Mining and Metallurgical Engineering, Yazd University, Yazd, Iran
1. Ph. D., 2. Associate Professor

DOI: http://10.22034/IJISSI.2026.2070586.1328
Published by ISSI (Iron & Steel Society of Iran)

the dual-phase ferrite–austenite region, followed by rapid quenching from the selected temperature [6].

The QP heat treatment is a novel and effective process for the design and production of the third generation of AHSS. The QP cycle consists of a four-step heating and cooling route: (1) austenitization, (2) rapid quenching in a molten salt bath to form a partial fraction of martensite along with austenite, (3) carbon partitioning from martensite into the adjacent austenite at higher isothermal temperatures to stabilize RA, and (4) rapid cooling in water or oil down to room temperature [7-11]. It is believed that with a smart design of the QP cycles, an enhanced combination of tensile strength and formability can be achieved [12].

The stabilization of RA is influenced by several factors, including the size of prior austenite grains, carbon concentration and alloying elements in the steel, lattice strain caused by tensile and compressive stresses, and morphology [13]. In the automotive industry, one of the key parameters in determining vehicle crash resistance is energy absorption capacity [14]. The product of tensile strength and uniform elongation is a reliable criterion for evaluating the balance between tensile strength and ductility in AHSS for engineering applications [15, 16]. Accordingly, in this research, the formation of micro-composite microstructures consisting of mixtures of retained austenite–martensite and ferrite–martensite, and their relationship with the mechanical properties of a medium-silicon low-alloy steel under QP heat treatment, are studied and compared with those obtained under SQ conditions.

2. Materials and Methods

The chemical composition of the 35CHGSA commercial-grade steel used in the present study is illustrated in Table 1. Heat treatments are carried out in electric resistance furnaces and molten salt baths. Critical temperatures, including the initial (Ac_1) and final (Ac_3) temperatures for austenite formation, as well as the martensitic transformation start (M_S) and finish (M_F) temperatures, are determined using dilatometry (Fig. 1.). The critical temperatures and the ranges of phase transformations are plotted using JMatPro 8.0 (Fig. 2.). To achieve uniform and homogeneous microstructures in the initial specimens, all samples were first austenitized at 900°C for 15min and then air-cooled to room temperature. To obtain the SQ specimens, the samples were reheated at 900°C for 15min and then held in a molten salt bath at 720°C for 5min. The QP heat treatment cycles consisted of heating to 900°C for 15min, primary quenching in a molten salt bath at 280°C, holding for 1 min to promote carbon partitioning, and finally quenching in water to room temperature. The heat treatment cycles employed in this study are schematically detailed in Fig. 3. Microstructural observations were carried out using a field-emission scanning electron microscope (FE-SEM, TESCAN-MIRA3). The distribution of different microphases was examined using EBSD analysis. Transmission electron microscopy (TEM) was conducted using a FEI Tecnai F20 microscope at 200kV. Thin foils (~3mm) were punched from 70μm thick foils and twin-jet electropolished in a solution

Table 1. Chemical composition of the investigated commercial grade of 35CHGSA steel (in wt.%).

C	Si	Mn	Cr	S	P	Mo	Ni	Ti	V	Fe
0.35	1.25	0.89	1.18	0.01	0.01	0.01	0.04	0.03	0.01	96.2

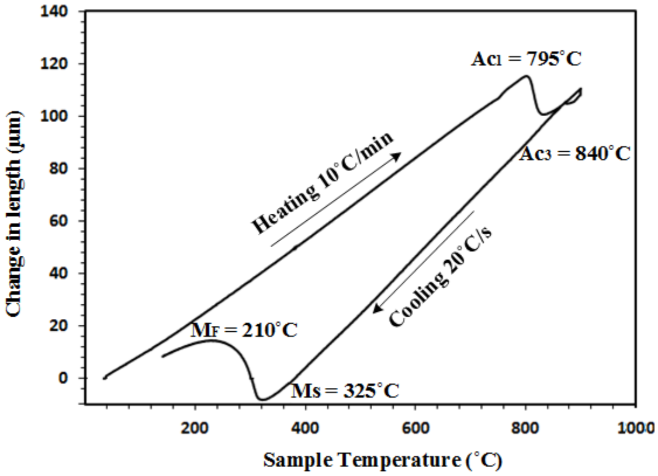

Fig. 1. The graph of changes in the length of the sample in terms of temperature resulting from the dilatometric thermal test in order to determine the critical temperatures on the 35CHGSA steel sample.

of 6% perchloric acid and 94% methanol at −20°C. Sample preparation was performed at room temperature using a voltage of 20kV and a current of 0.8 A for 15 to 60 seconds. X-ray diffraction (XRD) analysis was performed at room temperature using an Asenware AW-DX300 diffractometer with Cu-Kα radiation (λ = 0.1542nm). Vickers macrohardness measurements were conducted with a load of 30kg using a DIA-Testor 722 hardness tester. For tensile testing, three specimens were prepared in the rolling direction in accordance with DIN 50125 (2004-01), and the tests were performed on a SANTAM STM-150 universal testing machine. The reported tensile results represented the average values of these three specimens. Charpy impact specimens (55×10×5mm V-notch) were tested according to the ASTM A370 standard. To ensure reproducibility, three specimens were tested per heat treatment cycle, and the average impact energy was reported.

3. Results and Discussion

3.1. Electron Microscopy Observations

Fig. 4. illustrates the FE-SEM microstructures of the steel under QP in comparison with SQ. The microstructure of the SQ specimens consists of a mixture of ferrite, FM, and RA (Fig. 4a.), whereas the QP-treated specimens exhibit a mixture of CFTM, FM, and RA (Fig. 4b.). The initial martensite formed during direct quenching in the molten salt bath at 280°C is tempered during the 1-min partitioning step. This type of martensite, forming partially adjacent to the primary austenite regions, appears as blocky structures in the microstructure. During isothermal holding in the 280°C molten salt bath, carbon diffuses from the supersaturated martensite into the adjacent untransformed austenite, thereby increasing the carbon content of the austenite phase. This reduces the martensite start temperature

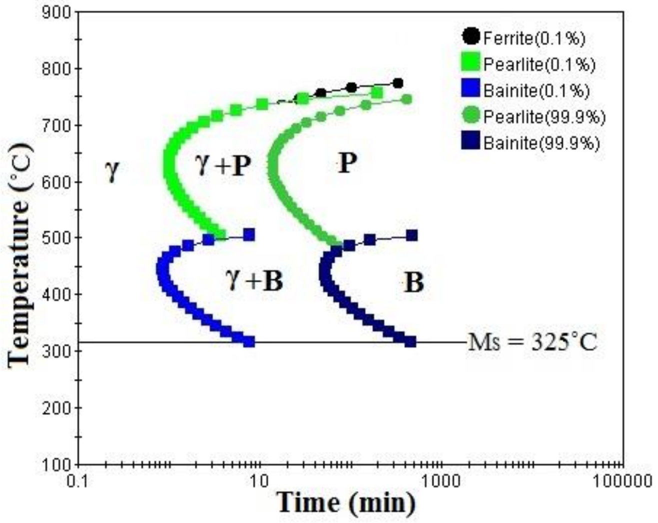

Fig. 2. Temperature-time-phase transformation (TTT) diagram of 35CHGSA steel used in the present study.

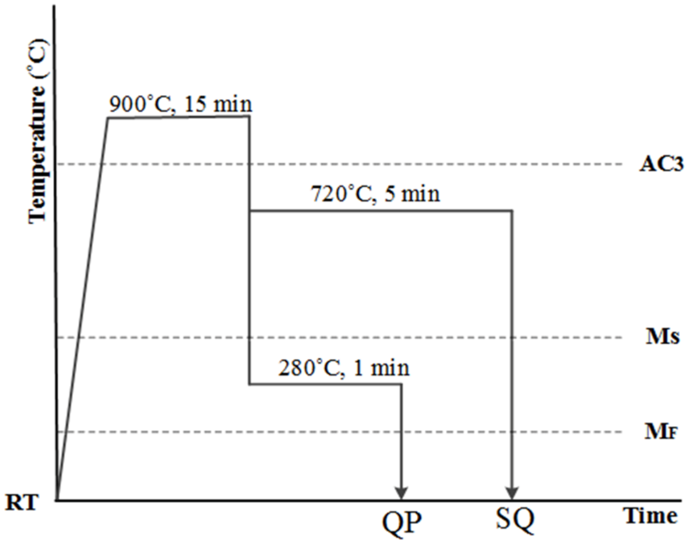

Fig. 3. Schematic diagrams of the heat treatment cycles used for SQ and QP samples.

(Ms) and facilitates the formation of fresh martensite/retained austenite. No evidence of carbide formation is observed in the QP specimens, which can be attributed to the effect of silicon in delaying carbide precipitation. Silicon, due to its insolubility in carbide phases, inhibits carbide formation during the partitioning heat treatment [17-19]. Additionally, silicon delays the transformation of unstable carbides from the first tempering stage (η or ε carbides) to stable cementite (Fe_3C) during the final tempering stage [20-22].

3.2. TEM Microstructural Observations

Fig. 5. displays TEM images of QP specimens in light and dark backgrounds using electron diffraction of the RA. The selected area electron diffraction pattern (SAEDP) is shown on the left and top of the light-background image, and the corresponding dark-background image is shown on the right, using electron diffraction of the RA. TEM investigations, including comparisons of dark- and light-field images and electron diffraction pattern analysis, indicated the formation of a soft phase in the RA among needle-shaped martensite crystals in DWQ samples. Further electron microscopy investigations of the microstructure of the QP samples revealed no carbide formation. The presence of 1.25wt.% silicon effectively prevented carbide formation, even with the presence of significant amounts of carbon (0.35wt.% carbon) at the relatively high partitioning temperature of 280°C.

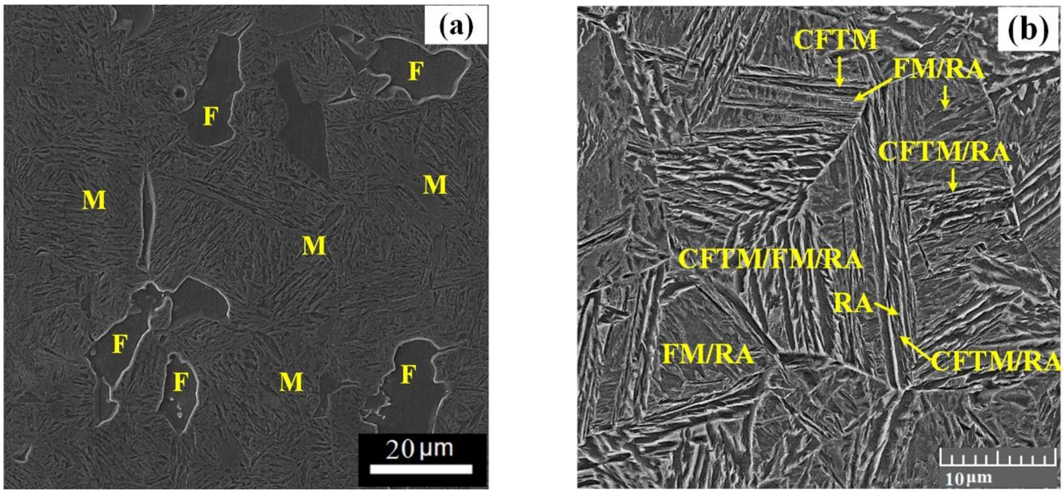

Fig. 4. Scanning electron microscopy images of the microstructures of: (a) SQ; (b) QP sample. The regions of ferrite, fresh martensite, tempered martensite, carbide-free tempered martensite, fresh martensite/retained austenite, and carbide-free tempered martensite/retained austenite are denoted by F, FM, TM, CFTM, FM/RA, and CFTM/RA, respectively.

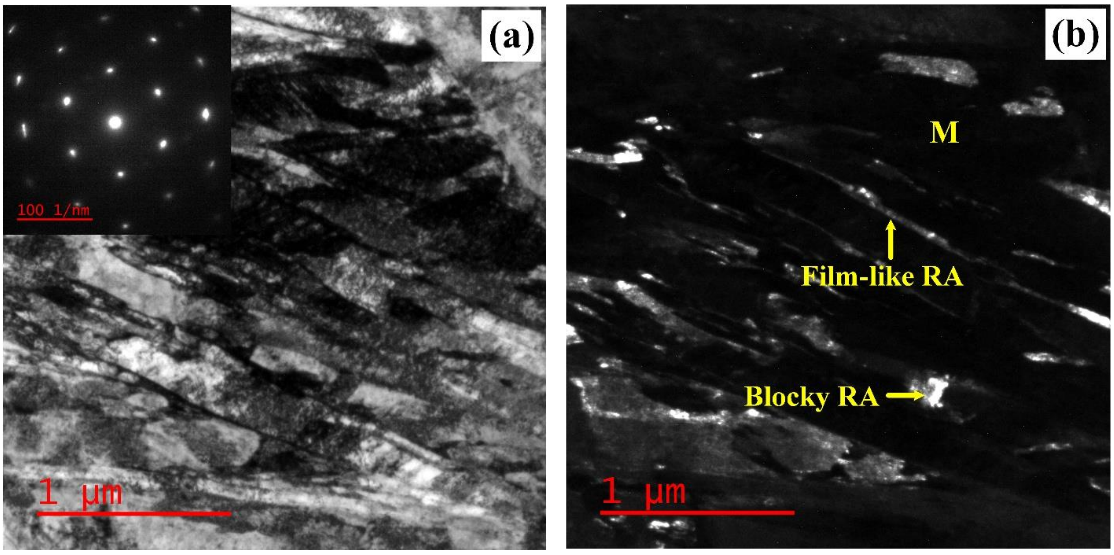

Fig. 5. Transmission electron microscope images of the microstructure of QP specimens. The Selected Area Electron Diffraction Pattern (SAEDP) of martensite and retained austenite is shown on the top left of the light background (a) and the corresponding dark background (b) on the right. Martensite regions are marked with the letter M.

3.3. EBSD Microstructural Observations

Phase distribution maps obtained from EBSD can be used to investigate the spatial distribution of phases within the microstructure. The phase analysis of SQ and QP specimens is presented in Fig. 6. As illustrated in Figs. 6a and 6b, the microstructure of the SQ specimens consists of martensite/ferrite phases (red). The images of the QP specimens reveal the presence of 97vol.% martensite (red) and 3vol.% retained austenite (RA, blue) after partitioning at 280°C for 1min (Fig. 6a and 6b.). At elevated partitioning temperatures, carbon diffusion into adjacent untransformed austenite regions is enhanced, further lowering the martensite start temperature (Ms) and thereby stabilizing retained austenite during the final rapid-cooling stage. Despite selecting a step size of 40nm for EBSD analysis, the quantitative determination of RA fractions in these specimens cannot be fully relied upon. During surface preparation, retained austenite may transform into martensite under mechanical loading, and thin RA films with thicknesses below 50nm cannot be detected. Another factor limiting the reliability of quantitative results is that the analyses are performed on very small regions, which may not represent the overall microstructure because of potential local heterogeneities.

3.4. Volume Fraction of Retained Austenite

Fig. 7. illustrates the X-ray diffraction (XRD) patterns of the QP specimens compared to the SQ specimens for a more comprehensive investigation. In the XRD patterns, the (110), (200), and (211) peaks correspond to martensite/ferrite, while the (111), (200), and (220) peaks are attributed to RA. The RA peaks are clearly distinguishable in the QP specimens. Based on peak intensities in the diffraction patterns and using the Rietveld method, the volume fraction of RA in the QP specimens was determined to be 7%, whereas the RA fraction in the SQ specimens was lower. These results indicate that partitioning facilitates significant carbon transfer from FM to adjacent austenite regions during holding in the molten salt bath at 280°C, thereby stabilizing a substantial amount of retained austenite in the final water-quenching step.

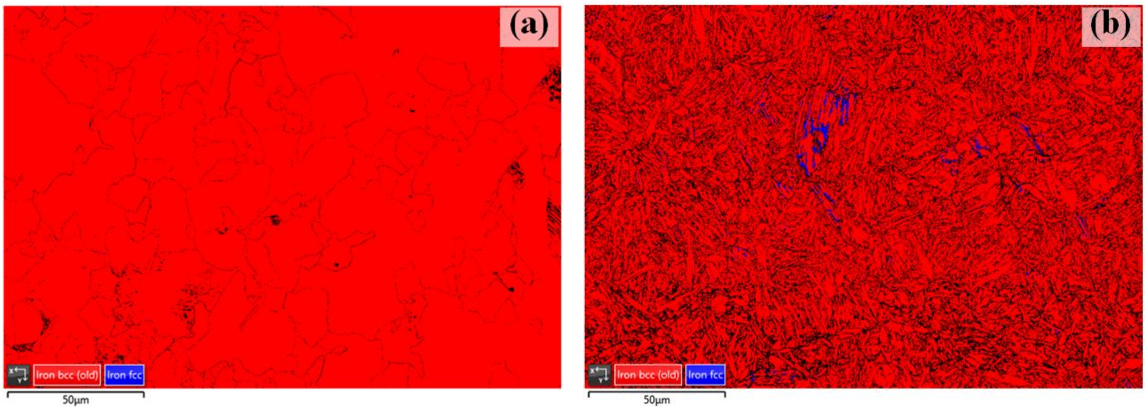

Fig. 6. Phase map images obtained from EBSD for the samples: (a) SQ; (b) QP. In these images, the red color indicates the martensite phase, while the blue color represents the retained austenite phase.

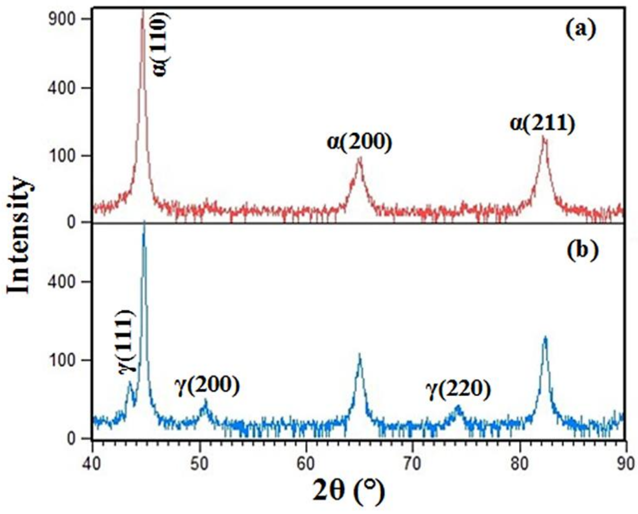

Fig. 7. X-ray diffraction (XRD) patterns of the samples subjected to (a) SQ in comparison with (b) QP treatment.

3.5. Tensile Properties

The engineering stress–strain curves of the SQ and QP specimens are compared in Fig. 8, and the average tensile properties are summarized in Table 2. According to the tensile results presented in Table 2., the SQ specimens exhibit a yield strength of 1290MPa, ultimate tensile strength (UTS) of 1353MPa, and the lowest total elongation (1.8%). The total elongation of the QP specimens increased significantly to 6.7%, while the yield strength was remarkably maintained above 1291MPa, and the UTS increased to 1592MPa. These results indicate that the QP-treated specimens possess an optimal combination of tensile properties compared with the SQ specimens, with the product of UTS and total elongation increasing significantly to a maximum of 10.2GPa·%. As previously mentioned, the product of UTS and total elongation (PSE) serves as a reliable criterion for evaluating the balance between tensile strength and ductility in advanced high-strength steels for engineering applications.

The notable improvement in the engineering properties of the QP specimens is attributed to the formation of a micro-composite microstructure comprising CFTM, FM, and RA. The formation of hard martensitic crystals contributes significantly to the strength enhancement of the QP specimens within a 1min partitioning time. At the same time, the soft, thin interlayered RA films play a key role in improving ductility. Specifically, these thin RA films located between hard martensitic crystals can hinder crack initiation and propagation during plastic deformation, thereby significantly enhancing toughness. Moreover, RA can partially transform into martensite during tensile testing, providing a TRIP effect that mitigates stress concentration, delays necking, and consequently increases both tensile strength and uniform elongation [23, 24].

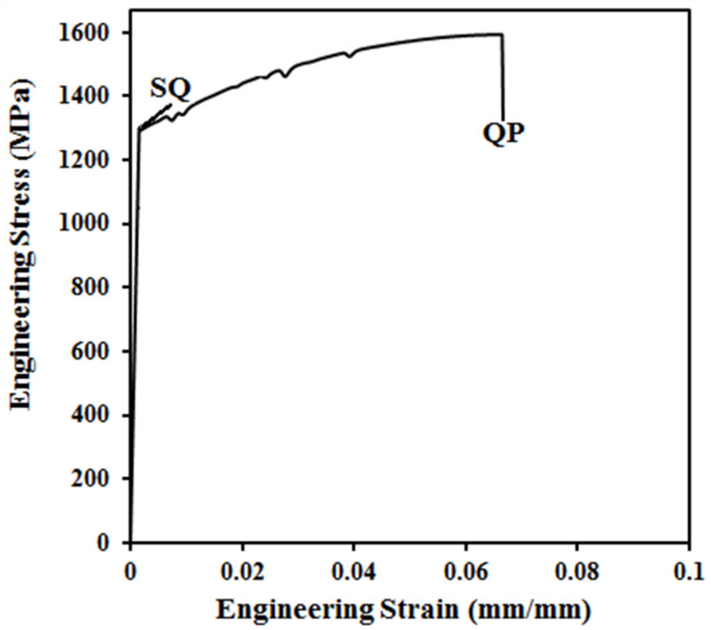

Fig. 8. Engineering stress–strain curves of the samples subjected to QP treatment compared with those of the SQ samples.

Table 2. Tensile strength, yield strength, uniform elongation, total elongation, and the product of tensile strength and uniform elongation obtained from tensile tests under quenching and partitioning heat treatment compared with step quenching.

Sample Characteristic	YS(MPa)	UTS (MPa)	UEL (%)	TEL (%)	UTS×UEL(GPa.%)
SQ	1290	1353	1.8	1.8	2.4
QP	1291	1592	6.4	6.7	10.2

3.6. Toughness

The comparison of the Charpy impact energy of the SQ and QP specimens is presented in Fig. 9. The results indicate a significant difference in Charpy energy absorption between the specimens. The SQ specimens exhibit a Charpy impact energy of 3.5J, whereas the QP specimens deliver a higher impact energy of 5.5J, indicating superior energy absorption (enhanced toughness). The remarkable increase in impact energy of the QP specimens is attributed to the formation of a micro-composite microstructure comprising fine needle-like martensitic crystals adjacent to soft RA. The thin RA films located between martensitic needles or laths act as barriers to crack initiation and propagation, thereby improving toughness and impact resistance, because the RA phase is softer and more ductile than the hard martensitic phase. In fact, the thin RA films positioned between hard martensitic crystals, oriented perpendicular to the crack propagation direction, reduced triaxial stress conditions at the crack tip and hindered crack growth [25, 26]. Moreover, retained austenite with an FCC crystal structure inherently exhibits greater plastic deformability and toughness than the hard BCT martensitic phase.

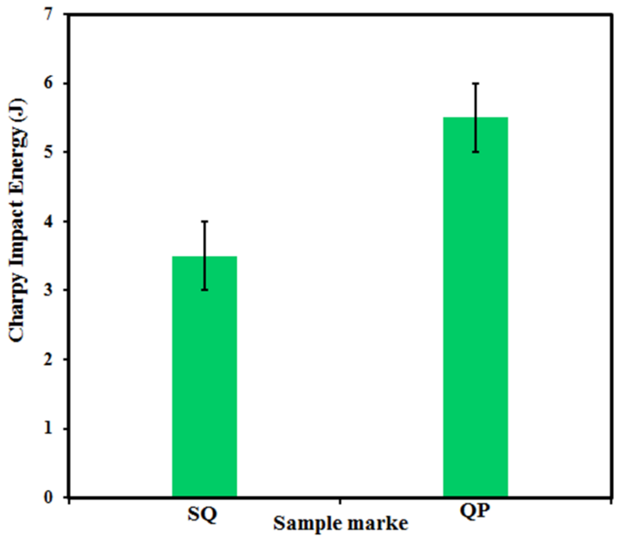

Fig. 9. Comparison of Charpy impact energies of the samples subjected to QP treatment with those of the SQ samples.

4. Conclusions

This study aimed to investigate the mechanical behavior of a medium-silicon low-alloy steel (Fe-0.35C-1.25Si-0.89Mn-1.18Cr) subjected to step quenching (SQ) and quenching and partitioning (QP) heat treatments. The main findings can be summarized as follows:

- The presence of 1.25wt.% Si along with 0.89wt.% Mn prevented carbide formation during the 1min partitioning process at 280°C.
- The total elongation of the QP specimens increased significantly from 1.8% (SQ) to 6.7%, while the yield strength remained unchanged at 1290MPa.
- The mechanical properties of the QP specimens were remarkably improved compared with the SQ specimens. The product of ultimate tensile strength (UTS) and total elongation for the SQ specimens was 2.4GPa·%, whereas it increased substantially to 10.2GPa·% for the QP specimens.
- The Charpy impact energy of the SQ specimens was 3.5J, while the QP specimens exhibited a higher impact energy of 5.5J, indicating superior toughness.

Acknowledgements

The authors would like to thank Dr. Grzegorz Cios (AGH University) for performing the EBSD analysis.

References

[1] Khajesarvi A, Banadkouki S, Sajjadi S, Somani M, Abnormal trend of ferrite hardening in a medium-Si ferrite-martensite dual-phase steel, Metals. 2023; 13(3): 542.
[2] Li K, Yang T, Gong N, Wu J, Wu X, Zhang D.Z, et al. Additive manufacturing of ultra-high strength steels: a review, J Alloys Compd. 2023; 171390.
[3] Venezuela J, Lim F.Y, Liu L, James S, Zhou Q, Knibbe R, et al. Hydrogen embrittlement of an automotive 1700 MPa martensitic advanced high-strength steel, Corros Sci. 2020; 171: 108726.
[4] Khajesarvi A, Ghasemi Banadkouki S, Sajjadi S, Effect of carbon partitioning on abnormal martensite hardening in a conventional quench and temper medium silicon low-alloy steel under ferrite-martensite dual-phase microstructure, HTM J Heat Treat Mater. 2023; 78(3): 141-161.
[5] Mohanty R, Girina O, Fonstein N, Effect of heating rate on the austenite formation in low-carbon high-strength steels annealed in the intercritical region, Metall Mater Trans A. 2011; 42(12): 3680-3690.
[6] Khajesarvi A, Ghasemi Banadkouki S.S, Somani M.C, Kömi J, Sajjadi S.A, Investigation of micromechanical properties of martensite and ferrite microphases in a 35CHGSA medium-Si low-alloy steel, Steel Res Int. 2024; 95: 2300624.
[7] Matlock D.K, Bräutigam V.E, Speer J.G, Application of the quenching and partitioning (Q&P) process to a medium-carbon, high-Si microalloyed bar steel, In: Materials Science Forum, Zurich: Trans Tech Publications. 2003; 426-432: 1089-1094.
[8] Speer J.G, Streicher A, Matlock D.K, Rizzo F, Krauss G, Quenching and partitioning: a fundamentally new process to create high-strength TRIP sheet microstructures, In: Austenite Formation and Decomposition, Warrendale (PA): TMS. 2003: 505-522.

[9] Rizzo F, Edmonds D.V, He K, Speer J.G, Matlock D.K, Clarke A.J, Carbon enrichment of austenite and carbide precipitation during the quenching and partitioning (Q&P) process. In: Proceedings of the International Conference on Solid-Solid Phase Transformations in Inorganic Materials. 2005: 535-544.
[10] Edmonds D.V, He K, Rizzo F, De Cooman B.C, Matlock D.K, Speer J.G, Quenching and partitioning martensite: a novel steel heat treatment, Mater Sci Eng A. 2006; 438-440: 25-34.
[11] Gerdemann F, Speer J.G, Matlock D.K, Microstructure and hardness of steel grade 9260 heat-treated by the quenching and partitioning (Q&P) process. Mater Sci Technol. 2004; 20: 439-449.
[12] Speer J.G, Matlock D.K, De Cooman B.C, Schroth J.G, Carbon partitioning into austenite after martensite transformation, Acta Mater. 2003; 51(9): 2611-2622.
[13] Xiong X, Chen B, Huang M, Wang J, Wang L, The effect of morphology on the stability of retained austenite in a quenched and partitioned steel, Scr Mater. 2013; 68(5): 321-324.
[14] Yusof N, Sapuan S.M, Sultan M.T.H, Jawaid M, Maleque M.A, Design and materials development of automotive crash box: a review, Cienc Tecnol Mater. 2017; 29(3): 129-144.
[15] Shiraiwa T, Kato S, Briffod F, Enoki M, Exploration of outliers in strength-ductility relationship of dual-phase steels, Sci Technol Adv Mater Methods. 2022; 2(1): 175-197.
[16] Li M, Hu X, Yan S, Liu X, The effect of annealing temperature and temper-rolling on microstructure, mechanical properties, and Lüders strain of Fe-0.25C-5.9Mn-1.0Al-1.57Si medium-Mn steel, Steel Res Int. 2023; 94(9): 2200924.
[17] Kumar R, Dwivedi R, Singh V.P, Kuriachen B, Krishnan N.A, Influence of toughness and retained austenite on wear behaviour of carbide-free bainite in high silicon steel, Trans Indian Inst Met. 2022: 1-10.
[18] Chang L, Microstructures and reaction kinetics of bainite transformation in Si-rich steels, Mater Sci Eng A. 2004; 368(1-2): 175-182.
[19] Khajesarvi A, Banadkouki S, Investigation of carbon and silicon partitioning on ferrite hardening in a medium silicon low-alloy ferrite-martensite dual-phase steel, Int J Iron Steel Soc Iran. 2020; 17(2): 25-33.
[20] Khajesarvi A, Ghasemi Banadkouki S.S, Sajjadi S.A, Effect of tempering heat treatment on mechanical properties of a medium silicon low-alloy ferrite-martensite dual-phase steel, Int J Iron Steel Soc Iran. 2022; 19: 20-29.
[21] Bramfitt B.L, Mangonon PL J.R, Metallurgy of continuous-annealed sheet steel, Proceedings of a conference; 1982 Feb 15-16; Dallas, TX. Warrendale (PA): Metallurgical Society of AIME. 1982.
[22] Nouri A, Kheirandish S, Saghafian H, Effect of silicon content on the strain hardening of dual-phase steels, Iran J Mater Sci Eng. 2008; 5(4): 40-49.
[23] Jacques P.J, Delannay F, Ladrière J, On the influence of interactions between phases on the mechanical stability of retained austenite in transformation-induced plasticity multiphase steels, Metall Mater Trans A. 2001; 32(11): 2759-2768.
[24] Saleh M, Priestner R, Retained austenite in dual-phase silicon steels and its effect on mechanical properties, J Mater Process Technol. 2001; 113(1-3): 587-593.
[25] Hertzberg R.W, Vinci R.P, Hertzberg J.L, Deformation and fracture mechanics of engineering materials, 6th ed. Hoboken (NJ): John Wiley & Sons; 2020.
[26] Khajesarvi A, Ghasemi Banadkouki S.S, Sajjadi S.A, Superior improvement of microstructure and mechanical properties of a medium silicon low-alloy 35CHGSA steel under quenching and partitioning heat treatment in comparison to conventional quenching and tempering condition, J Metall Mater Eng. 2022; 33(2): 73-91.